Thermoelectric heat recovery in a real industry: From laboratory optimization to reality

Álvaro Casi[a], Miguel Araiz[a], Leyre Catalán[a], David Astrain[a,*]

[a]*Department of Engineering, Institute of Smart Cities, Public University of Navarre, Pamplona, Spain*

Abstract

Thermoelectricity, in the form of thermoelectric generators , holds a great potential in waste heat recovery, this potential has been studied and proved in several laboratory and theoretical works. By the means of a thermoelectric generator, part of the energy that normally is wasted in a manufacturing process, can be transformed into electricity, however, implementing this technology in real industries still remains a challenge and on-site tests need to be performed in order to prove the real capabilities of this technology. In this work, a computational model to simulate the behaviour of a thermoelectric generator that harvest waste heat from hot fumes is developed. Using the computational model an optimal configuration for a thermoelectric generator is obtained, also an experimental study of the performance of different heat pipes working as cold side heat exchangers is carried out in order to optimize the performance of the whole thermoelectric generator, thermal resistances of under 0,25 K/W are obtained. The optimized configuration of the thermoelectric generator has been built, installed and tested under real conditions at a rockwool manufacturing plant and experimental data has been obtained during the 30 days field test period. Results show that 4.6 W of average electrical power are produced during the testing period with an efficiency of 2.38 %. Moreover, the computational model is validated using this experimental data. Furthermore, the full harvesting potential of an optimized designed that takes advantage of the whole pipe is calculated using the validated computational model, resulting in 30.8 MWh of energy harvested during a sample year which could meet the demand of 8.34 Spanish average households.

Keywords: Thermoelectric generator, computational model, passive heat-exchangers, on-site experimentation, waste-heat

1. Introduction

Global energy demand increases each year and most of it is covered by the use of fossil fuels [1]. The excessive use of these fuels causes multiple environmental issues, such as global warming, rising sea levels, oil spills, ocean acidification or acid rain [2, 3]. These problems, alongside the inevitable depletion of the fossil fuel resources, establish the current energy situation, which might be one of the biggest challenges humanity has to face on the 21st century [4].

In 2018, 32.31 % of the energy produced in the United States was transformed into energy services, while the missing 67.68 % of the energy was rejected [5]. Most of this rejected energy comes as waste heat that is dissipated directly to the atmosphere and 37 % of it is estimated to arise at temperatures above 100 °C [6]. This vast amount of wasted thermal energy can be recovered by a wide amount of technologies, such as recuperators, regenerators, economisers, Organic Rankine cycles, piezoelectric systems or thermoelectricity [7]. Pourkiaei et al. presented a review of thermoelectric applications and concludes that the heat source of thermoelectric generators (TEGs) is supplied from free or cheap resources, such as waste heat [8]. Zabeb et al. reviewed solid state generators for waste heat recovery and stands that the most promising sector to implement these systems is the processing industry, reducing the primary energy consumtion while saving resources [9].

Thermoelectricity, in the form of TEGs, produces energy by taking advantage of a heat flow and is capable of exploiting this large amount of thermal energy that is currently being wasted. Thermoelectric modules (TEMs) are the main elements of TEGs and they transform heat into electricity by taking advantage of the Seebeck effect [10]. Temperature gradient at the thermoelectric module (TEM) determines the amount of power that can be harvested, the greater the temperature gradient, the greater the electrical energy that can be obtained. In order to maximize this gradient, heat exchangers are used at both hot and cold sides of the TEMs, approaching the temperature of the hot side of the TEM to the hot sink and the cold side of the TEM to the cold sink. Aranguren et al. proved that the performance of the heat exchangers greatly affects power output [11]. In further studies, Aranguren et al. concluded that auxiliary consuption becomes a critical factor for the production of electricity in thermoeelectric generators [12]..

Several experimental studies have been carried out integrating a phase change heat exchanger in a thermoelectric generator (TEG). Kumar et al. built a thermoelectric power generation system using a thermosyphon and studied opperating parameters [13]. Catalán et al. developed a thermoelectric generator with phase change heat exchangers to obtain an autonomous vigilance station at Teide volcano [14]. Deng et al. managed to effectively recycle waste heat produced in coalfield subsfaces fires using a thermoelectric generator with heat pipe based heat

*Corresponding author at: Engineering Department. Public University of Navarre, Campus de Arrosadia s/n, 31006 Pamplona, Spain.
Email address: david.astrain@unavarra.es (David Astrain)

Nomenclature

Variables

A	Area	m^2
c_p	Specific heat at constant pressure	$J/kg \cdot K$
$Data$	Value of the data	
E	Electromotive force	V
e	Thickness	m
$Error$	Value of the error	
I	Current	A
k	Thermal conductivity	$W/m \cdot K$
Nu	Nusselt number	
Pr	Prandtl number	
$\dot{Q}$	Heat flux	W
$\bar{q}$	Volumetric heat generation	W/m^3
R	Thermal resistance	K/W
R_0	Electric resistance of the material	Ω
Re	Reynolds number	
T	Temperature	K
V	Voltage	V
$\dot{V}$	Volumetric flow	m^3/s
W	Electrical power	W
ΔT	Temperature gradient	K
α	Seebeck coefficient	V/K
η	Efficiency	
π	Peltier coefficient	V
ρ	Density	kg/m^3
σ	Thomson coefficient	V/K

Subscripts

A	Metal A
amb	Ambient
B	Metal B
c	Cold side of the thermoelectric module
chx	Cold side heat-exchanger
$cond$	Conduction
$cont$	Contact
$conv$	Convection
cop	Copper pins
cu	Copper
$evap$	Evaporator
exp	Experimental
ext	Extracted
fum	Fumes
gen	Generated
h	Hot side of the thermoelectric module
hhx	Hot side heat-exchanger
i	Block number of the pipe
im	Interface material
ins	Insulation
$Joule$	Due to the Joule effect
n	N doped thermoelectric material
opt	Optimized simulation
p	P doped thermoelectric material
$Peltier$	Due to the Peltier effect
rel	Relative
s	Surface
sim	Simulated
sup	Power supply
tem	Thermoelectric module
$Thoms.$	Due to the Thomson effect

Abbreviations

HX	Heat exchanger
TEG	Thermoelectric generator
TEGs	Thermoelectric generators
TEM	Thermoelectric module
TEMs	Thermoelectric modules

exchangers [15]. Therefore, passive heat exchangers that lack auxiliary consumption such as heat pipes or thermosyphons in natural convection have become a suitable option for different thermoelectric applications [16].

The potential of this technology at the industrial sector has been calculated in several theoretical case studies. Meng et al. studied recycling exhaust gas sensible heat through a TEG that would produce 1.47 kW with a 4.5 % efficiency [17]. Yazawa et al. proposed heat recovery from waste heat in a glass melting process in which an optimally designed thermoelectric system could generate 55.6 kW of electricity with a 15 % efficiency [18]. Elonkawan et al. results showed that 172.3 kW with a 4.3 % efficiency can be recovered from a 50 m lenght duct [19]. Araiz et al. proposed transforming waste-heat from a hot gas flow into electricity, resulting in a maximum net power of 45.8 kW, besides, the Levelised Cost of Electricity, LCOE, is studied for this technology, resulting in competitive results within current energy sources [20].

These thermoelectric theoretical works show great potential for waste heat recovery but laboratory and field test studies need to be performed to prove the capabilities of this technology. Nesarajah and Frey, managed to produce 2 W of power from an exhaust pipe under laboratory conditions [21]. Remeli et al. were able to produce 7 W of electrical power in a lab scale bench-top prototype with passive heat-exchangers [22]. Aranguren et al. managed to produce up to 24 W of electrical power from an exhaust of a combustion chamber that heats up water [23]. This sort of laboratory tests and experiments give valuable information in thermoelectric generation applications but, field studies under real conditions need to be performed in order to evaluate the viability of this technology at the industrial sector. In one of the few field studies regarding this topic, Børset et al., managed to obtain 160 W/m^2 in the casting area of a silicon plant absorbing heat via radiation and predicted that with some improvements 900 W/m^2 could be obtained [24]. However, these studies do not focus on the heat exchanger configuration or performance and do not use passive heat exchangers, which present many advantages and have been proved suitable for this applications. Besides, configuration of a TEG is yet to be discussed and tested on-site in a manufacturing plant.

The main objective of this work is to develop a small-scale passive TEG suited for waste heat recovery at a rockwool production factory and perform test field studies of the generator overtime. In order to do that, a computational model that simulates the behaviour of the TEG is developed and an optimization via the computational model is performed to help with the designing process. An optimized configuration is obtained built, installed and tested under real conditions at a manufacturing plant acquiring experimental data over 30 days. Besides, after experimental data is obtained, the computational model is validated. Finally, by the means of the computational model, the true harvesting potential of a large-scale TEG is calculated for a sample year.

The outline of this paper is as follows: In section 2 the location and conditions of the TEG are exposed and the methodology of this work is described. In section 3 an optimization of the TEG is performed and the setup of the prototype is described. In section 4 the experimental results are presented and the computational model is validated. In section 5 the harvesting potential of an optimized configuration is obtained. Finally, discussions are made and conclusions are drawn.

2. Methodology

The followed methodology starts with the development of a computational model that simulates the behaviour of a TEG that harvest waste heat from hot fumes. Then, a small scale prototype is designed using the computational model alongside an experimental study on the performance of the cold side heat exchangers. The optimized configuration of the prototype is built, installed and tested at a rockwool manufacturing plant. Using the collected experimental data the computational model is validated and to conclude, the real harvesting potential of an optimized configuration that takes advantage of the whole flow of hot fumes is calculated.

The development and design of a TEG varies greatly on the location to exploit, thus, the location of the prototype is selected first. In this case, the prototype is meant to be installed in a rockwool manufacturing plant, taking advantage of the waste heat produced during the manufacturing process. Alongside this process, high amount of waste heat is produced in the form of hot fumes and several places present thermal energy being dissipated directly to the atmosphere, where, thermoelectric generators can be installed to harvest energy. Besides, the location and design of the prototype needs to be addressed from a practical point of view, taking into consideration multiple criteria that is left behind in theoretical works and laboratory prototypes.

The location of the prototype is selected regarding the temperature of the fumes, the volumetric flow, accessibility and disruption of the process. In general, the greater the temperature and the volumetric flow of the fumes, the greater the harvesting potential. After analysing different exploitable areas throughout the manufacturing process a location is selected. The selected location consists of a pipe with a diameter of 0.9 m where fumes flow at 340 °C with a volumetric flow of 30 000 Nm^3/h. As it can be seen in Figure 1, the pipe is provided with a manhole used for maintenance purposes, where, the TEG will be mounted. The pipe is surrounded by a 200 mm layer of insulation to maintain the exterior of the pipe at low temperatures due to safety reasons. This location comes with a constant flow of high temperature fumes which provides a reliable heat source and the manhole gives accessibility without any disruption or modification of the process.

A structure that fits in the manhole hollow space has been designed and constructed, this frame is able to support a TEG and serves as a manhole for maintenance purposes. The structure is made of stainless steel and is mounted to the pipe by the use of 8 bolts of 12 mm. The void left in the structure is then filled with rockwool in order to preserve the isolation purposes of the pipe.

The design idea of the prototype consists of a hot side heat exchanger that extracts as much thermal energy as possible from the fumes to the outside of the pipe where the TEMs are

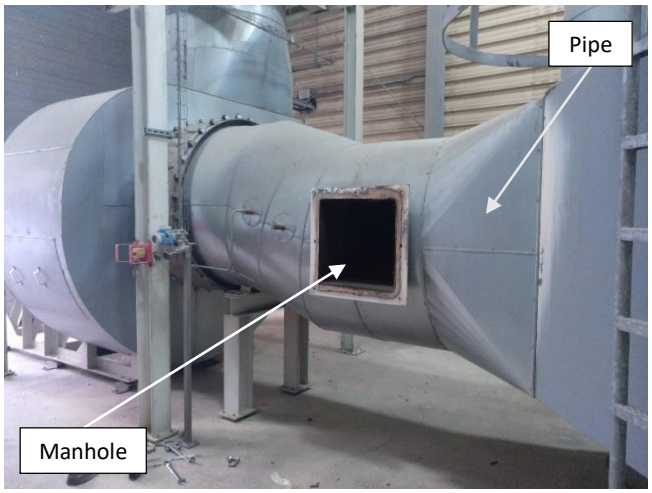

Figure 1: Location of the prototype

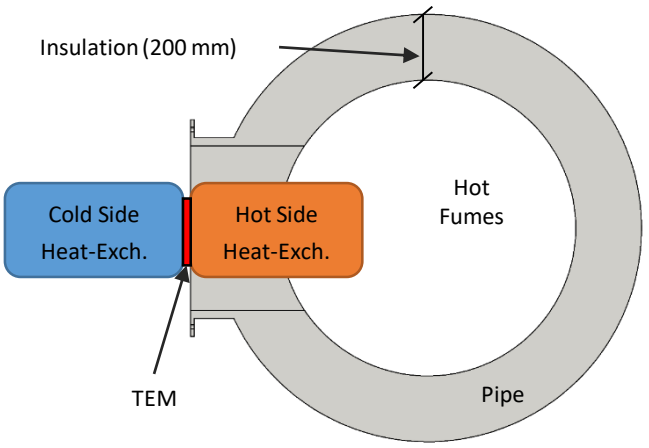

Figure 2: Schematic of the installation

located. On the TEMs, part of the thermal energy is transformed into electricity, while the rest is dissipated to the ambient through the cold side heat exchangers. For this purpose, the 200 mm layer of isolation that surrounds the pipe is set as an extra inconvenient, diminishing the energy harvesting potential. A schematic of the prototype in its location can be seen in Figure 2.

The proposed hot side heat exchanger consists of an electrolytic copper bar that transport the heat through the insulation layer by conduction. Copper pins are disposed to enhance the convection with the hot fumes in the interior of the pipe. The section of the copper bar is 60 mm × 60 mm and the pins diameter is 6 mm due to constructive reasons. The number of pins is maximized to increase the convective area and the length of the pins is set at 250 mm in order to not disrupt the production process. 23 pins are attached to the copper bar in a staggered configuration to enhance heat transfer [25]. The length of the copper bar will depend on the cold side heat exchangers, allowing a proper attachment. TG12-08-01LS modules from Marlow industries are used. These commercial modules, with a ZT of 0.73, are 40 mm × 40 mm × 3.5 mm and are able to work at temperatures up to 225 °C in steady state conditions [26]. As Aranguren et al. remarked, the auxiliary consumption affects greatly net energy production in TEGs, therefore, passive heat exchangers such as heat pipes or thermosyphons are better suited for this application [12]. In this case, heat pipe based heat exchangers with no auxiliary consumption to pump the liquid have been selected for the cold side. An in depth experimental optimization of said heat exchangers is described in subsection 2.2.

2.1. Computational model

The computational model simulates the behaviour of a TEG that harvest waste heat from hot fumes, obtaining power generated by the TEMs, heat flow and temperature distribution across the generator. This model is based on a previously published model and has been adapted for this application [27, 28]. It is coded in Matlab and based on the finite-differences implicit method under the assumption of unidirectional heat transfer. The TEG is discretized in 17 nodes as it is shown in Figure 3, including the heat source (hot fumes), the heat sink (ambient), the heat exchangers (hot and cold side) and the TEMs (junctions, ceramics and thermoelectric material).

The hot fumes are represented by node 1 and the ambient by node 17. The hot side heat-exchanger corresponds to nodes 2 and 3 while the cold side heat exchanger is represented by node 16. Finally the TEM is defined from nodes 4-15, node 4 and 15 represent the hot and cold ceramic plate of the TEMs respectively and nodes 3-14 define the thermoelectric material and the junctions.

The convective thermal resistance between the hot fumes and the copper pins ($R_{conv\,hhx}$) is calculated using Zukauskas correlation for predicting the heat transfer in staggered tube banks showed in Equation 1 [25].

$$Nu_{conv\,hhx} = 0.8 \cdot Re^{0.4} \cdot Pr^{0.36} \cdot \left(\frac{Pr}{Pr_s}\right)^{0.25} \tag{1}$$

Heat conduction thermal resistance through the copper bar ($R_{cond\,hhx}$) is estimated using Equation 2 [29].

$$R_{cond\,hhx} = \frac{e_{cu}}{k_{cu} \cdot A_{cu}} \tag{2}$$

The thermal contact resistances between the TEMs and the heat exchangers ($R_{cont\,h}$ and $R_{cont\,c}$) depend on the contact interface material properties as Equation 3 shows [29].

$$R_{cont\,h} = R_{cont\,c} = \frac{e_{im}}{k_{im} \cdot A_{im}} \tag{3}$$

From node 4 to 15 the TEM is represented and all the thermoelectric phenomena (the Peltier, Seebeck, Thomson and Joule effects) along with the Fourier Law are taken into account as in Equations 4 - 9 [27, 28].

$$\alpha_{AB} = \frac{dE}{dT} = \alpha_A - \alpha_B \tag{4}$$

$$\dot{Q}_{Peltier} = \pm\pi_{AB} I = \pm IT(\alpha_A - \alpha_B) \tag{5}$$

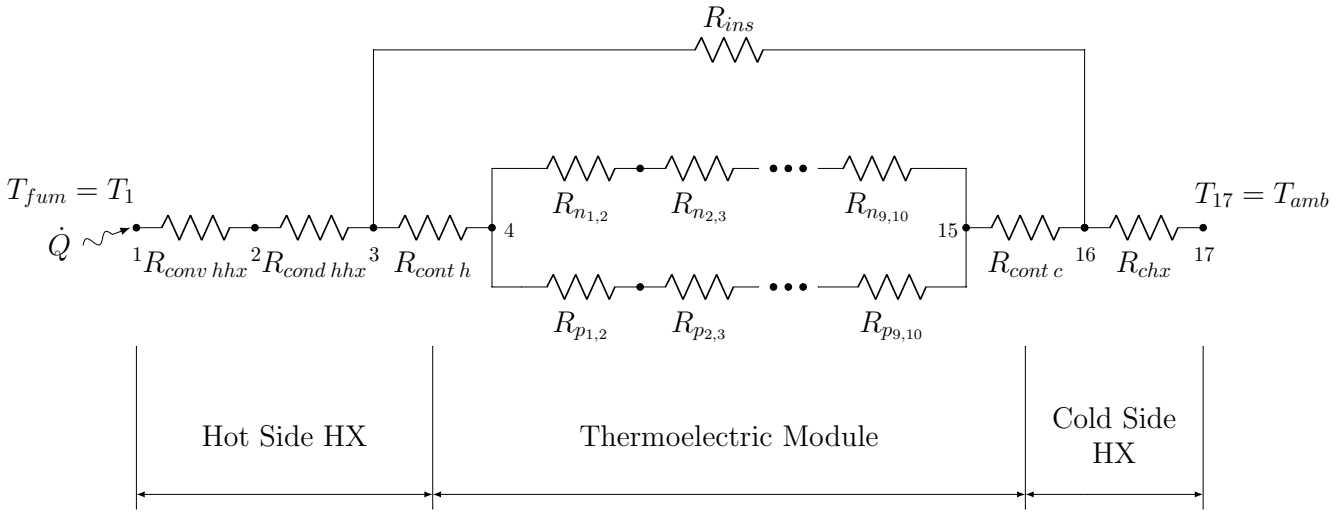

Figure 3: Thermal-electric analogy of the TEG computational model to harvest waste heat from hot fumes

$$\dot{Q}_{Thoms.} = -\sigma \overrightarrow{I}(\overrightarrow{\Delta T}) \tag{6}$$

$$\dot{Q}_{Joule} = R_0 I^2 \tag{7}$$

$$\rho c_p \frac{\partial T}{\partial t} = k\left(\frac{\partial^2 T}{\partial x_2} + \frac{\partial^2 T}{\partial y_2} + \frac{\partial^2 T}{\partial z_2}\right) + \bar{q} \tag{8}$$

The thermal bridge that appears at the insulation between the hot side heat exchanger and the cold side heat exchanger (R_{ins}) is also introduced in the computational model as Equation 9 shows [29].

$$R_{ins} = \frac{e_{ins}}{k_{ins} \cdot A_{ins}} \tag{9}$$

Regarding the cold side heat exchangers, an experimental optimization of passive heat exchangers is performed and described in subsection 2.2. Therefore, the thermal resistance of the cold side heat exchanger (R_{chx}) is introduced as a polynomial second order function of the heat flux as in Equation 10, obtained by experimental results.

$$R_{chx} = a + b \cdot \dot{Q}_{chx} + c \cdot \dot{Q}^2_{chx} \tag{10}$$

2.2. Cold side heat exchangers

Heat pipe based heat exchangers, under natural convection, are tested at greater length as cold side heat exchangers for the TEG. A heat pipe is a two phase heat transfer device, it consists of a sealed tube filled with a working fluid that transports heat through phase change, also, the interior of the pipe is covered with a wick structure [30]. Their working principle is as follows: the evaporator absorbs heat from the heat source, vaporizing the water inside the pipes, vapour ascends to the condenser zone through the tubes, here, heat is dissipated while vapour turns into liquid, finally, the liquid returns to the evaporator zone by gravity and capillarity effects across the wick structure closing the cycle.

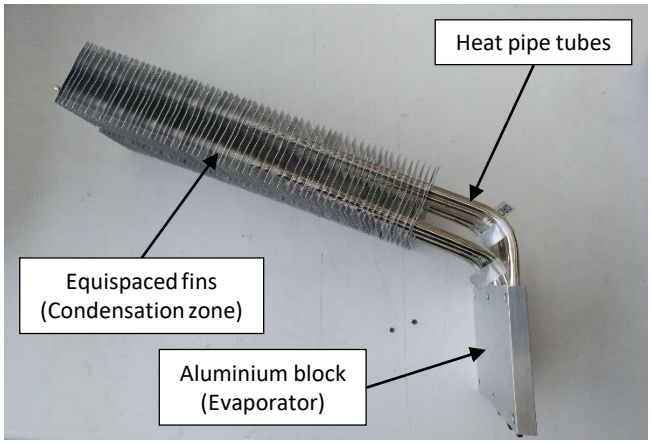

Figure 4: Groove 5 mm fin spacing heat pipe heat exchanger

Each heat pipe based heat exchanger consists of 8 tubes made of cooper, the length of each tube is 500 mm with an exterior diameter of 8 mm. They are filled with water as working fluid and two types of wick structure are tested: metal sintered powder (Sinter) and grooved wick (Groove). The first 100 mm of the tubes are embedded in an aluminium block that works as the evaporator, where the heat is absorbed. Along the rest of the tube, the condensation zone, equispaced fins are disposed. In order to test the effect of the fin spacing, 4 different distance between fins are tested: 3, 5, 7 and 9 mm. These heat exchangers are designed for 2 TEMs each (they can also be used for 1 or 3 TEMs as they also fit on the evaporation surface), Figure 4 shows one of the heat exchangers tested.

To evaluate the performance of the heat exchangers, and select the ones that performe best for this application, they are tested under laboratory conditions. As a heat source, 2 blocks of copper of 40 mm × 40 mm × 10 mm are used, each block of copper contains 6 cartridge heaters and covers the exact same area as a TEM. The cartridges are connected electrically in parallel to an adjustable DC electric power supply. The cooper

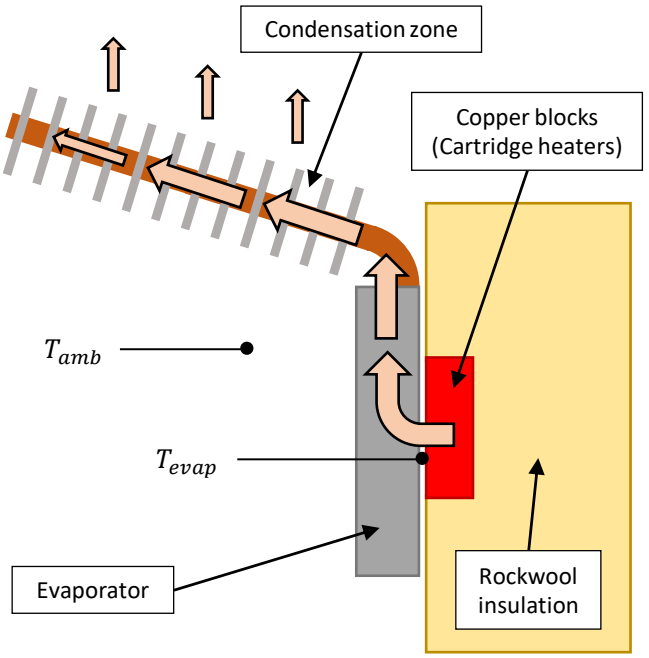

Figure 5: Cold side heat exchangers test configuration schematic

Table 1: Resolution and accuracy of the sensors used

Sensor	Resolution	Accuracy
Ahlborn T 190-0 NiCr-Ni (°C)	0.1	±0.5
Ahlborn ZA 9900 AB3 DC (V)	0.01	±0.02
Ahlborn ZA 9900 AB4 DC (V)	0.1	±0.2
Ahlborn ZA 9901 AB4 DC (A)	0.01	±0.02

blocks are placed at the evaporator, corresponding to the aluminium block. In order to ensure that all the heat produced in the cartridges flows through the heat exchanger, all free surfaces of the copper blocks are insulated with rockwool layers. Ahlborn T 190-0 NiCr-Ni thermo-wires are disposed at key points to measure temperature, the voltage and the current supplied to the heaters are measured using Ahlborn ZA 9900 AB4 DC voltage and Ahlborn ZA 9901 AB4 DC current measuring modules. An Ahlbron Almemo 5690 data acquisition system is used. Resolution and accuracy of the sensors used are listed in Table 1. In Figure 5 a schematic of the test configuration is presented. The arrows in the schematic represent heat flow during the tests. All the tests are performed under natural convection conditions.

In this study, 4 different distances between films (3, 5, 7 and 9 mm) and 2 types of wick structure (Sinter and Grooved) had been tested. The thermal resistance parameter, shown in Equation 11, is used to evaluate the performance of the heat exchanger. Evaporator temperature (T_{evap}) and Ambient temperature (T_{amb}) sensors are disposed as Figure 5 shows, the heat flux through the heat exchanger ($\dot{Q}_{chx}$) is equal to the electrical power supplied by the DC electric power supply, as, all the electric power is transformed into heat and, the insulation ensures

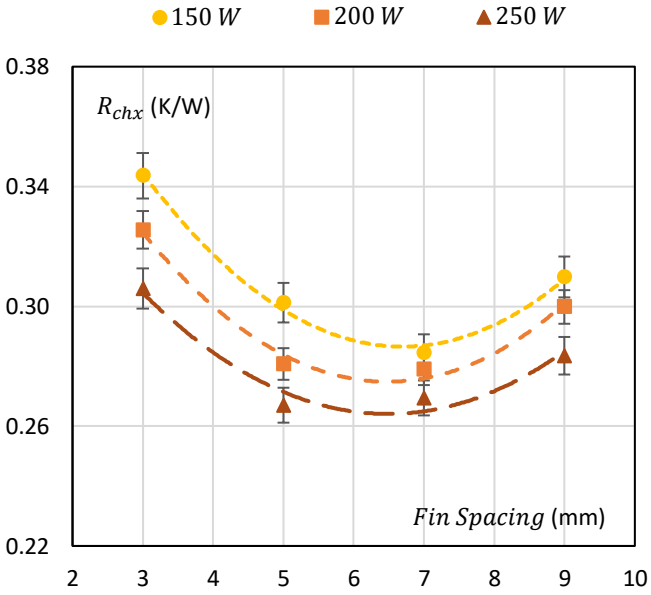

Figure 6: Thermal resistance of a Groove type pipe heat exchanger as a function of the fin spacing distance for different heat fluxes. Curves are second-order polynomial fits of data points

that the heat produced at the cartridges flows only through the heat pipe heat exchanger. Therefore, the heat flux is obtained as Equation 12.

$$R_{chx} = \frac{T_{evap} - T_{amb}}{\dot{Q}_{chx}} \tag{11}$$

$$\dot{Q}_{chx} = W_{sup} = V_{sup} \cdot I_{sup} \tag{12}$$

Figure 6 shows thermal resistances obtained during the tests for the different distances between fins for Groove pipes, the heat inputs selected are 150, 200 and 250 W. Three replicas of every configuration have been carried out and the overall uncertainty range is calculated an included in the figures. Firstly, the thermal resistance decreases when the heat increases for each one of the fin spacing configurations. This effect was expected, as an increase in heat flux contributes to a higher temperature of the pipes, thus increasing the pipe-to-ambient temperature gradient and enhancing the heat transfer in natural convection conditions. Short fin spacing involves an increase of the convection area which benefits the heat transfer coefficient, in contrast, when fins are too close to each other air does not flow freely between fins and heat transfer diminish. Therefore, a balance between these two factors needs to be obtained.

Thermal resistance seems to have an optimal value between 5 and 7 mm fin spacing, depending on the heat flux, whereas for 3 mm, thermal resistance increases due to air flow reduction and, for 9 mm, resistance enlarges as the convective area drops. Noteworthy is the huge rate of improvement for 5 mm fin spacing when heat flow grows, the thermal resistance diminish 13.8 % when increasing heat from 150 to 250 W. This effect can be explained when airflow between the fins acts as a bottleneck. For low heat inputs, natural convection is not able to generate a decent natural draft, in contrast, for high heat fluxes,

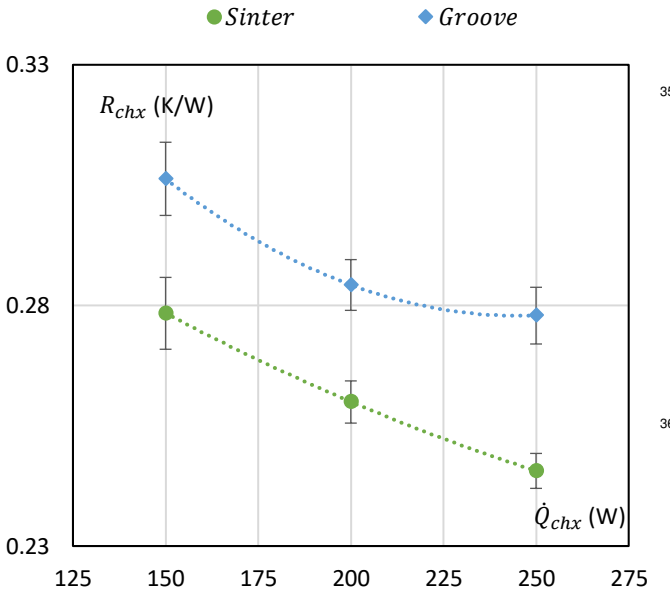

Figure 7: Thermal resistance for Groove and Sinter type pipes as a function of the heat flux for 5 mm fin spacing. Curves are second-order polynomial fits of data points

the pipe-to-ambient temperature difference increases, enhancing natural draft and eliminating this bottleneck, therefore, all the extra convective area provided by the fins starts to be effective, resulting in a significant decrease in thermal resistance. In summary, each fin spacing is optimal for a range of heat input. In this case, from 150 to 200 W, the optimal is set on 7 mm fin spacing, whereas from 200 to 250 W, a separation of 5 mm provides better results. The data obtained clearly shows that a separation between 5 and 7 mm is the optimal for this configuration, 5 mm has been set as the fin separation for the rest of this work, as high heat fluxes are expected.

Heat exchangers with Groove and Sinter wick type had also been tested, both of them with 5 mm spacing. The heat inputs tested correspond to 150, 200 and 250 W. Results obtained can be seen in Figure 7 alongside the overall uncertainty range (three replicas of every configuration have been carried out). As anticipated, thermal resistance diminish for higher heat fluxes, confirming the tendency for both pipe types. As heat flux increases, temperature difference between the heat exchanger and the ambient increases, enhancing natural convection. This effect is clearly visible in Sinter type pipes, where thermal resistence decreases almost linearly with the heat flux. However, in Groove type pipes thermal resistance becomes asymptotic beyond a heat flux value of 225, this means, another effect is limiting the Groove type pipe for higher heat fluxes. This can be explained as the return of liquid through the grooved canals is not sufficient for high heat fluxes. For Sinter type pipes, this effect will also appear for even higher heat fluxes. Groove pipes performed 11.21, 9.53 and 13.41 % worse than Sinter pipes for 150, 200 and 250 W heat fluxes respectively. Following these results, sintered powder heat pipes with 5 mm fin separation are presented as an optimal solutions for the cold side and had been selected as cold side heat exchangers for the prototype for the rest of the work. The polynomial second order function that is introduced in the computational model can be seen in Equation 13.

$$R_{chx} = 0.35 - 6.49 \cdot 10^{-4} \cdot \dot{Q}_{chx} + 8.04 \cdot 10^{-7} \cdot \dot{Q}^2_{chx} \quad (13)$$

3. TEG optimization and setup

In this section an optimal configuration for the TEG is obtained using the developed computational model. Then, the optimal configuration is built and the description of the prototype setup is presented.

3.1. Optimal configuration

An optimization study of the whole TEG is performed using the computational model described in subsection 2.1. The number of heat exchangers and TEMs used to built a TEG affects drastically the performance of a TEG in multiple aspects. Using just 1 TEM per heat exchanger means all the heat that passes through the thermoelectric module is dissipated by a whole heat exchanger and therefore the heat dissipation is optimal, this produces a high temperature gradient at the TEM which means larger power produced per module. In contrast, if more TEMs are placed in one heat exchanger heat dissipation decreases for each module resulting in lower temperature gradients at the TEMs and therefore lower power outputs per module. Therefore, an optimization between low number of TEMs with high power outputs and larger number of TEMs with low power outputs needs to be performed in order to maximize the total output power. With this study an optimal configuration of the elements for this TEG under the expected conditions will be obtained.

The number of hot side heat exchangers to use is set to 1 and the parameters to optimize are the number of TEMs and the number of cold side heat exchangers that will be used to built the TEG. Ambient temperature is set at 25 °C and fumes temperature is set at 340 °C. The number of cold side heat exchangers is simulated from 1 to 4 and the number of TEMs is introduced related to the amount of cold side heat exchangers, 1, 2 or 3 TEMs can be attached to each cold side heat exchangers and therefore, multiple configurations appear. The length of the hot side heat exchanger will be modified during the simulations as a larger number of cold side heat exchangers means a longer copper bar to attach the heat exchangers. Power produced, heat extracted from the fumes, temperature gradient at the TEMs and efficieny of the TEMs are the outputs obtained during the simulations.

The simulated results obtained are summarized in Table 2. Also, Figure 8 shows an schematic of configurations 1, 2, 5 and 12 for a clearer understanding. Data obtained shows that when the number of TEMs for each cold side heat exchanger increases the total heat extracted by the TEG increases. As expected, as more TEMs are used the amount of heat through each TEM reduces and therefore temperature gradient at the TEMs decreases. This means lower power output is obtained

Table 2: Simulated configurations of the TEG

Config.	Nº of Cold side HX	Nº of TEMs / Cold side HX	TEMs	$\dot{Q}$ (W)	$\dot{Q}_{tem}$ (W)	ΔT_{tem} (°C)	η_{tem} (%)	W_{gen_tem} (W)	W_{gen} (W)
1	1	1	1	162.56	162.56	134.32	2.48	4.03	4.03
2	1	2	2	195.22	97.61	101.07	2.45	2.39	4.78
3	1	3	3	213.33	71.11	80.51	2.17	1.55	4.64
4	2	1	2	218.68	109.34	100.96	2.35	2.57	5.13
5	2	2	4	252.31	63.08	70.13	2.04	1.29	5.16
6	2	3	6	269.40	44.90	53.64	1.71	0.77	4.60
7	3	1	3	210.37	70.12	67.80	1.79	1.26	3.77
8	3	2	6	231.83	38.64	44.41	1.43	0.55	3.32
9	3	3	9	242.01	26.89	33.02	1.15	0.31	2.78
10	4	1	4	225.62	56.40	55.90	1.55	0.88	3.50
11	4	2	8	244.66	30.58	35.75	1.19	0.37	2.92
12	4	3	12	253.43	21.12	26.29	0.94	0.20	2.39

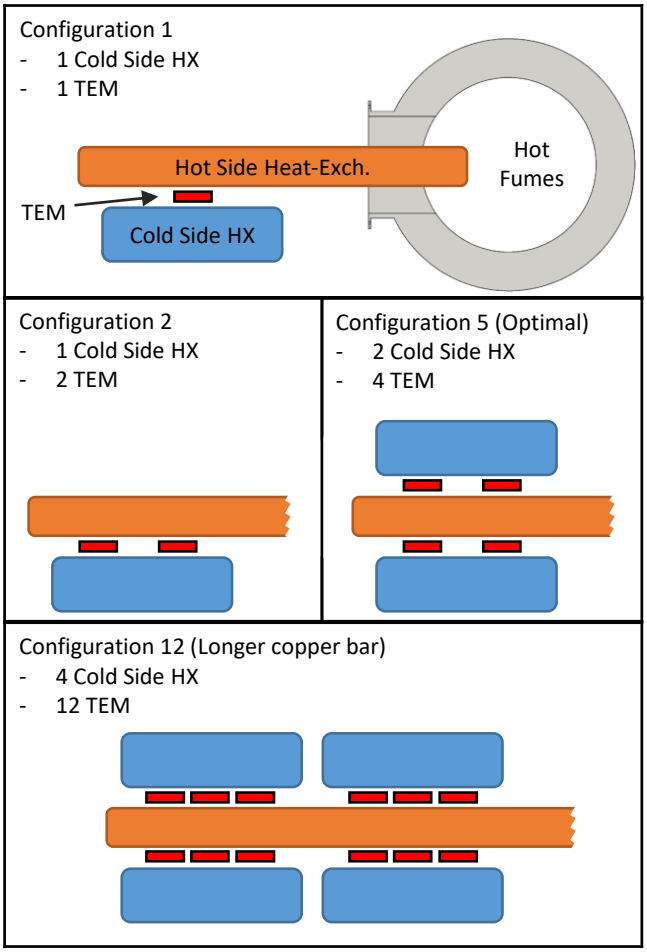

Figure 8: Schematic of configurations 1, 2, 5 and 12 from Table 2

per TEM, hence, for a set number of cold side heat exchanger an optimal number of TEMs is obtained. For 1 and 2 cold side heat exchangers the optimum power output is set at 2 TEMs per cold side heat exchangers, whereas for 3 and 4 cold side heat exchanger the optimum is obtained with 1 TEM per heat exchanger.

The effect of using more cold side heat exchangers also takes into account the necessity of a longer copper bar to attach the cold side heat exchangers. Increasing the length of the copper bar means lower heat extraction as the heat conduction thermal resistance (Equation 2) increases. In Figure 8 configuration 12 shows how the increase of the copper bar provides extra space for more thermoelectric modules and cold side heat exchangers. Although, when increasing the number of cold side heat exchangers, heat dissipation at the cold side improves and therefore, more heat is extracted. An optimum between both these phenomena is obtained with 2 cold side heat exchangers where the amount of heat extracted by the TEG is optimum.

The simulations show that an optimum power output of 5.22 W is obtained using 2 cold side heat exchangers and 2 TEMs per cold side heat exchanger. This configuration (highlighted in Table 2) is built and installed at the rockwool manufacturing plant as described in subsection 3.2. Worth to notice is that this configuration focuses on maximizing total output power with a resulting efficiency of 2.04 % which is not the maximum efficiency obtained during the simulations.

3.2. *Prototype setup*

The TEG consists of: a solid copper bar with pins working as hot side heat exchanger, 4 Marlow TG12-08 TEMs [26] and 2 heat pipe heat exchangers for the cold side, as the ones described in subsection 2.2. To attach these elements 6 mm bolts are used connecting both cold side heat exchangers, generat-

ing pressure across the TEMs and the copper bar, hence, ensuring reliable thermal contacts across the TEG, a detailed picture of the attachment is shown in Figure 9. In adition, heat extenders are disposed between the copper bar and the TEMs, these heat extenders are made of a solid aluminium block of $40\,\text{mm} \times 40\,\text{mm} \times 10\,\text{mm}$. The purpose of these heat extenders is double, first, they provide a clear path for the heat to the TEMs diminishing possible thermal bridges, and secondly, both faces of the block are mechanized with a small groove that allows thermocouples to be installed. The prototype is attached to the manhole structure filled with rockwool to preserve the isolation of the pipe, on the external end the prototype is isolated with rockwool and neoprene to avoid heat loss around the TEMs area. The prototype, displayed in Figure 9, is mounted on to the pipe during a programmed maintenance stop as Figure 10 shows.

TEMs are connected electrically in series, optimum load resistance varies from $2.9\,\Omega$ to $3.46\,\Omega$, depending on the hot and cold side temperatures of the TEM [26]. 3 resistances of $4.7\,\Omega$ had been connected in series resulting in a $3.525\,\Omega$ load resistance for each TEM. Ahlborn ZA 9900 AB3 DC voltage and Ahlborn ZA 9901 AB4 DC current measuring modules are disposed to obtain the energy produced by the TEMs. A total of 18 Ahlborn T 190-0 NiCr-Ni thermo-wires are disposed along the TEG as temperature sensors. Two of them monitor the temperature of the fumes, two are disposed at the copper pins, four at the exterior end of the copper bar, four at the hot side face of the TEMs, another four at the cold side face of the TEMs and the last two monitor the atmospheric temperature on the exterior of the pipe. All the sensors are connected to an Ahlborn Almemo 5690 data acquisition system storing the data in a computer. Resolution and accuracy of the sensors used in the prototype are listed in Table 1. For the initial restart of the manufacturing process data is acquired in 10 s intervals, after that, one measurement is made each 6 min. This experimental setup is designed to acquire thermoelectric generation data during the manufacturing process and test the performance of the system in a field test study, by the means of the DC voltage and DC current measuring modules the electrical power can be calculated directly.

4. Results and discussion

The prototype is installed for 30 days during summer season at the industrial plant. Throughout this period temperature across the prototype and power generation data have been acquired.

4.1. Prototype results

Figure 11 shows the temperature distribution obtained across the prototype and the power generated from the restart of the process until steady state conditions at the process are reached and therefore, reliable data can be acquired. On the 16th day, temperature and power generated drops drastically due to a programmed maintenance stop of the manufacturing process where the flow of hot gases stops and therefore the heat source that powers the TEMs disappears. On average, the fumes (T_{fum}) reach a temperature of 337.6 °C, part of the thermal energy carried by the fumes is absorbed by the copper pins, resulting in a temperature of 281.0 °C at the base of the pins (T_{cop}), where the copper bar starts. Alongside the copper bar a temperature drop of 147.6 °C takes place, resulting in 133.4 °C at the hot side face of the TEMs (T_h). At the TEMs a temperature gradient of 70.8 °C takes places, thus 62.6 °C are obtained at the cold side face of the TEMs (T_c), this gradient determines the power generated. Finally, the ambient temperature (T_{amb}) around the prototype averages 34 °C. Figure 12 shows this average temperature distribution on the prototype (Orange).

For the purpose of producing as much energy as possible, temperature gradient at the TEM must be as high as feasible, in order to achieve that, temperature gradient at both hot and cold side heat exchangers must be decreased to its minimum. As Figure 12 shows, temperature gradient at the hot side heat exchanger ($\Delta T_{hhx} = T_{fum} - T_h$) is quite noticeable (204.2 °C), in contrast, temperature drop at the cold side heat exchanger ($\Delta T_{chx} = T_c - T_{amb}$) is really small (28.6 °C). The hot side heat exchanger absorbs heat from the fumes via convection and transports it to the TEMs due to conduction, Figure 12 clearly shows that temperature drop during the convection ($T_{fum} - T_{cop} = 56.6\,°\text{C}$) is not as noticeable as temperature drop at the copper bar ($T_{cop} - T_h = 147.6\,°\text{C}$) and that this extraction of heat alongside de copper bar highly diminishes the harvesting potential. In subsection 5.2 the real potential of this technology is calculated when the TEMs can get closer to the pipe and the copper bar diminishes its lenght, this corresponds to the optimized simulation data (Blue) that appears in Figure 12. On the other side, the small temperature gradient at the cold side heat exchangers (ΔT_{chx}) proves that the heat pipe based heat exchangers optimized in subsection 2.2 had performed properly under real conditions.

The TEG produces an average of 4.6 W of electrical power (W_{gen}) with a 70.8 °C temperature gradient (ΔT_{tem}) between its faces, the peak power reaches up to 6.1 W during the night of the coldest day when ambient temperature decreases to its minimum, resulting in a 78.5 °C gradient at the TEMs. The average efficiency of the TEMs (η_{tem}) under this working conditions is 2.38 %, this efficiency is obtained as Equation 14 shows. Heat that pass through the TEMs ($\dot{Q}_{tem}$) is equal to: power generated plus the heat that is dissipated to the atmosphere by the cold side heat exchangers. The relation is shown in Equation 15, power generated is obtained directly through the data whereas heat dissipated to the atmosphere is obtained via an iterative calculation. To perform this iterative process temperature gradient and thermal characterization of the cold side heat exchangers are needed. Temperature gradient is obtained through the data and the thermal characterization has already been performed during the optimization of the cold side heat exchangers in subsection 2.2. Figure 7 shows thermal resistance as a function of the heat flux that passes through the heat exchanger, this curve is adjusted to a polynomial function, where the thermal resistance can be obtained directly if heat flux is introduced. The iterative process goes as follows: First, in order to start the iterations, heat flux through the heat exchanger is supposed, this

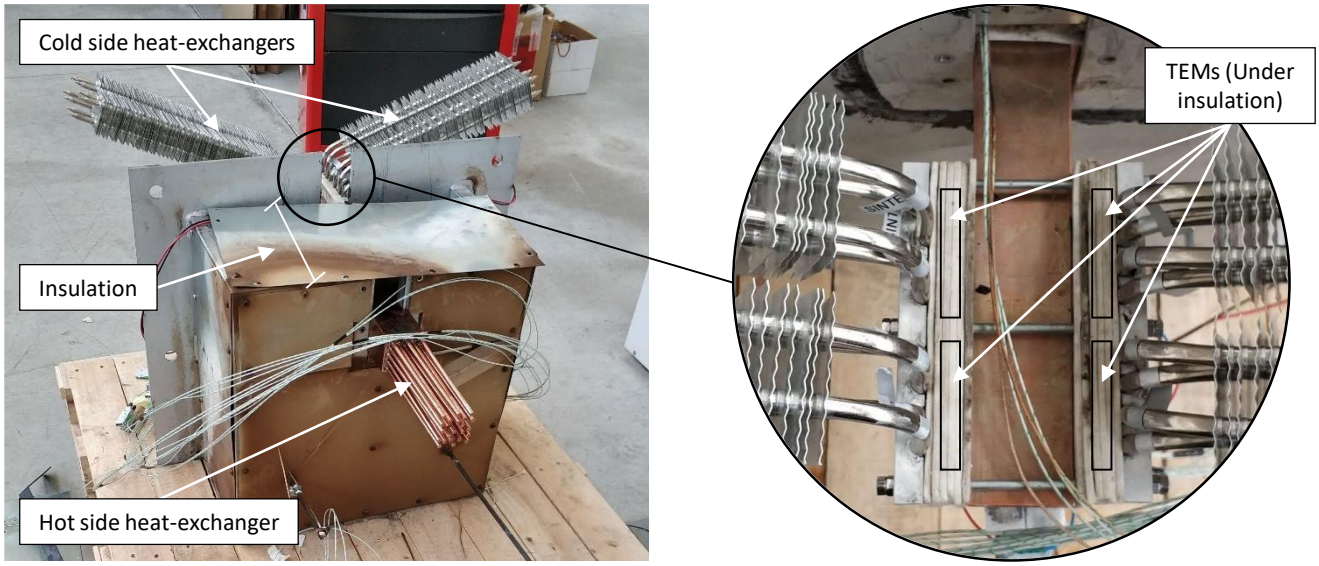

Figure 9: Thermoelectric generator prototype with detail of the attachment between heat exchangers and TEMs

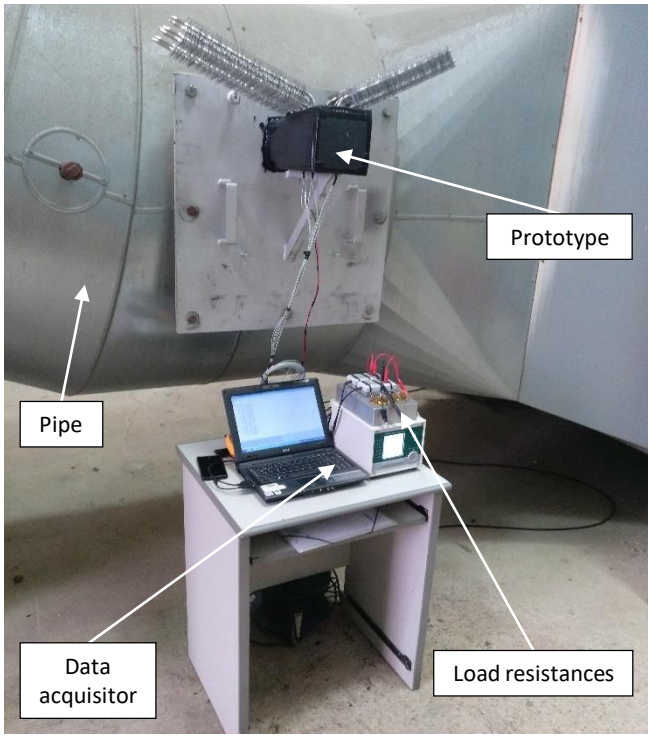

Figure 10: Thermoelectric generator and measuring equipment at the industrial plant

supposed heat flux is used to obtain thermal resistance of the heat exchanger using the adjusted polynomial function. This thermal resistance alongside the temperature gradient is introduced in Equation 11, obtaining heat flux through the cold side heat exchangers for the first iteration. With this heat flux, another iteration is performed until the results obtained and the heat introduced in the last iteration do not differ. Using this method a heat flux of 94.35 W is obtained for each heat exchanger, thus, 188.7 W cross both heat exchangers and 193.3 W pass through the TEMs resulting in an efficiency of 2.38 %.

$$\eta_{tem} = \frac{W_{gen}}{\dot{Q}_{tem}} \cdot 100 \tag{14}$$

$$\dot{Q}_{tem} = \dot{Q}_{chx} + W_{gen} \tag{15}$$

Temperature conditions change during each day and depend drastically on the season, affecting the TEG performance. The prototype has been tested during summer season when ambient temperature around the TEG reaches up to 43.7 °C at midday and drops to 23.7 °C at night. At night, when ambient temperature drops, the gradient on the TEMs increases from 66.5 °C to 75.5 °C, resulting in 3.8 W and 5.1 W of electrical power respectively, 34 % more energy is produced during the night on a sample day. Performance also varies between days, on the hottest day an average of 4.2 W are produced while in a cold day it reaches up to 5.2 W. During the testing period of the TEG, ambient temperature slowly decreases over the days. This traduces in an upward trend of the temperature gradient at the thermoelectric generator and therefore, an increase in power generation that can be appreciated in Figure 11.

4.2. Model validation

Using the experimental data obtained, the reliability of the model to simulate this TEG is tested. For that, after setting all the geometric values of the TEG, field data of fumes and atmo-

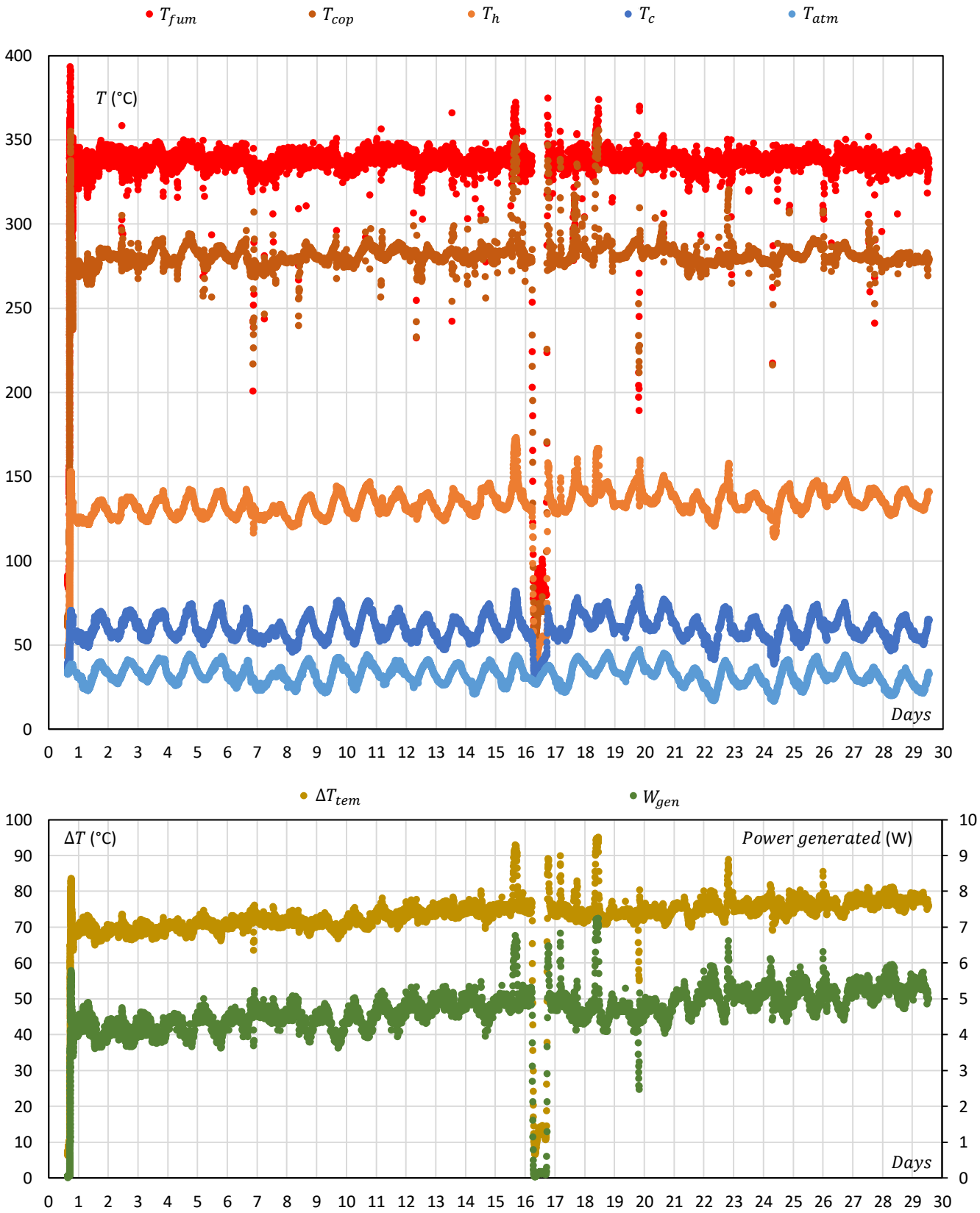

Figure 11: Temperature distribution and power generated across the prototype during the 30 days period

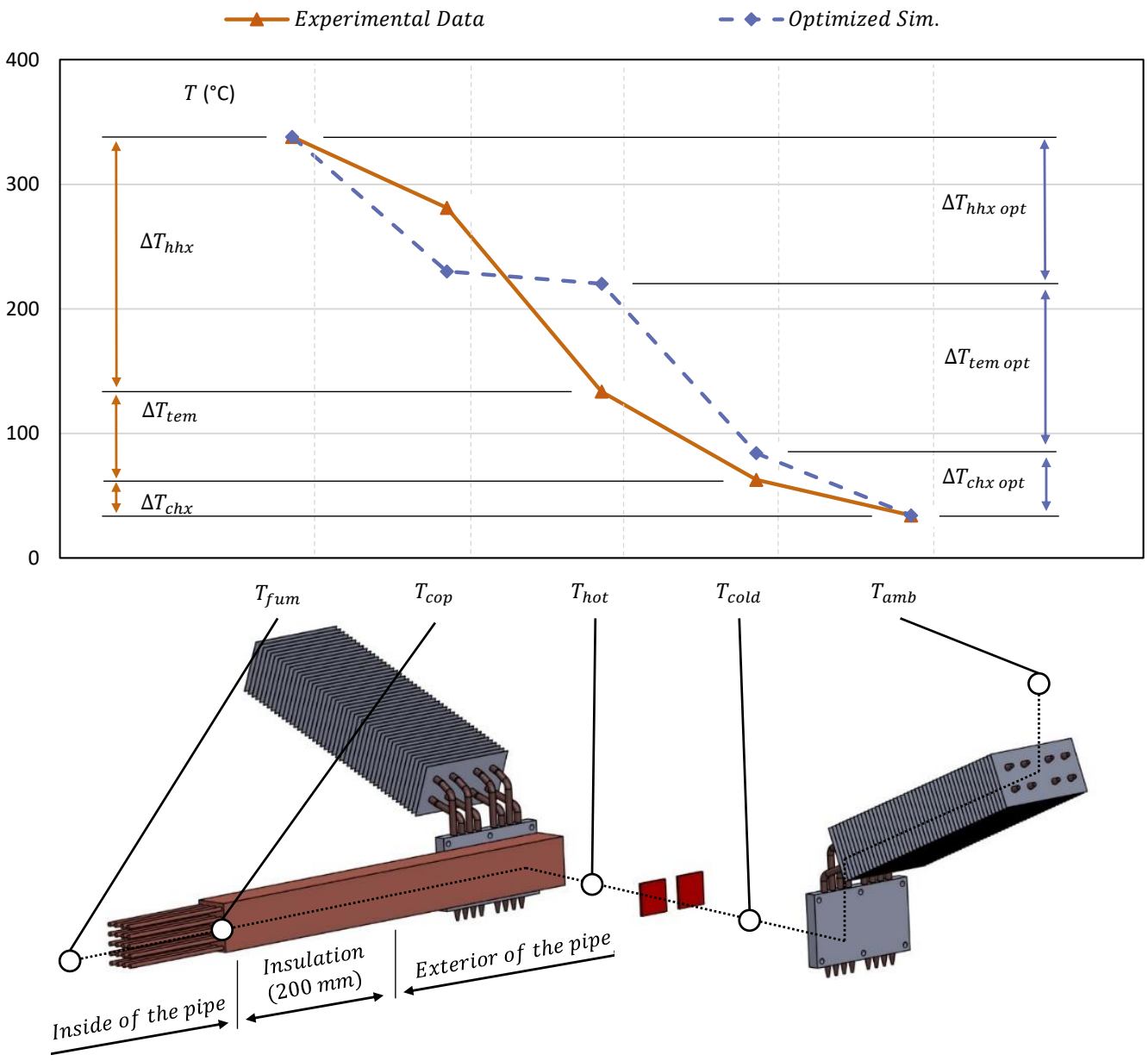

Figure 12: Average temperature distribution across the prototype during the testing period (Orange) and simulated temperature distribution of an optimized configuration (Blue)

spheric temperature are introduced on the computational model as inputs during one sample day. Data is introduced for each half hour, resulting in 48 simulations. The results obtained with the computational model are compared with field tests data. In Figure 13 simulated data is represented on top of the experimental data. As it can be seen, the simulated data does not differ much from the data obtained experimentally. The relative error ($Error_{rel}$) is calculated for the temperature gradient and the power generated at the TEM as Equation 16 shows.

$$Error_{rel} = \frac{Data_{sim} - Data_{exp}}{Data_{exp}} \cdot 100 \tag{16}$$

A statistical analysis of the relative error is made considering the values to follow a normal distribution, the mean and the standard deviation are calculated. The average relative error for the temperature gradient at the TEM is $-2.18\,\%$ with a standard deviation of $-2.33\,\%$, for the power generated, the average is $-1.05\,\%$ and the standard deviation sets at $4.48\,\%$. Besides, as it is shown in Figure 14 most of the relative error is within the $\pm 10\,\%$ range. As it has been proved that the model reliably represents what happens in the TEG, it can be used to obtain information in a larger scale setup.

5. Harvesting potential

In this section, using the TEG computational model developed in subsection 2.1 and validated in subsection 4.2 different scenarios are calculated. First, the harvesting potential of the current prototype at the current location is obtained during a sample year. Secondly, the harvesting potential of an optimized TEG at the current location is calculated during a sample year. And finally, the harvesting potential of an optimized TEG that takes advantage of the whole pipe at the current location is obtained.

5.1. Actual configuration

A whole year of energy harvesting with the current configuration at the current location is simulated. For that, the atmospheric and fumes temperature are introduced as inputs. The atmospheric temperature is obtained from the official meteorology and climatology website of the region [31] and corresponds to a weather station situated in the surroundings of the manufacturing plant, atmospheric data is available every hour. Fumes temperature also shifts during the day as Figure 11 shows, thus, fumes temperature is introduced as a changing value using the data obtained during the field tests.

The results obtained with the current configuration are summarized here: the TEG (4 TEMs) would be able to produce 45.16 kWh of energy during the whole year with 5.16 W of average total output power.

5.2. Optimized design

The prototype installed at the manufacturing plant extracts heat from the inside of the pipe through an insulation layer of 200 mm, this produces an average temperature drop of 147 °C and thus, reduces the harvesting potential of the TEG. However, if the design would be made from scratch or modifications to the location would be possible, that layer of insulation would not be present and therefore, the hot side of the thermoelectric module would be closer to the heat source, increasing its temperature, and therefore, its power generated. By the means of the computational model the harvesting potential over a sample year at the current location without the isolation is calculated. For that, as in subsection 5.1, atmospheric and fumes temperature are introduced as inputs. However, in this case, the length of the hot side heat exchanger copper bar is reduced to 120 mm, the minimum necessary to attach the TEMs.

Figure 12 shows average temperature distribution across the TEG during the simulations for this optimized design (Blue). With the reduction of the copper bar the temperature drop on the hot side heat exchanger (ΔT_{hhx}) decreases drastically from 204.2 °C to 108.4 °C, increasing the temperature gradient at the TEMs from 70.8 °C to 120.06 °C and therefore, increasing the energy produced. The results show that power generated increases a 145.58 % from the actual configuration resulting in 110.90 kWh of energy throughout the year. Average power output sets at 12.66 W with a temperature gradient of 120.06 °C at the TEM and an efficiency of 2.93 %.

5.3. Real potential

The TEG installed at the manufacturing plant and the optimized design are low scale systems to harvest energy from a pipe where hot fumes flow and only use a little part of the pipes surface to harvest energy. In this section, a computational study of the optimized design described in subsection 5.2 to take advantage of the whole pipe at the current location is performed using the computational model. The length of the pipe is 4.8 m and, with an square section whose side was 0.8 m the maximum amount of optimized TEG that would be able to fit on the outside of the pipe would be 288. To run the simulations, atmospheric and fumes temperature are introduced as inputs. Although, as much more energy is been taken from the fumes, in this case, the temperature drop of the fumes is taken into consideration. For that, the length of the pipe is discretized in 24 different blocks, power extracted on each block is subtracted from the fumes and temperature for the next level is obtained as shown in Equation 17.

$$T_{i+1} = T_i - \frac{\dot{Q}_{ext\,i}}{\dot{V}_{fum} \cdot \rho_{fum\,i} \cdot c_{p\,fum\,i}} \tag{17}$$

The whole system would consist of 288 optimized TEGs taking advantage of a 4.8 m lenght pipe with an exterior surface of 15.36 m^2, each optimized TEG uses 1 hot side heat exchanger, 2 cold side heat exchangers as the ones described in subsection 2.2 and 4 TEMs. Alongside the 4.8m length pipe the system would only decrease the temperature of the fumes from 340 °C to 326.82 °C, this low temperature decrease of the fumes means that with the proposed system the fumes flow is not drastically affected, hence, much more energy could be extracted if the length of the pipe could be extended and more TEGs could

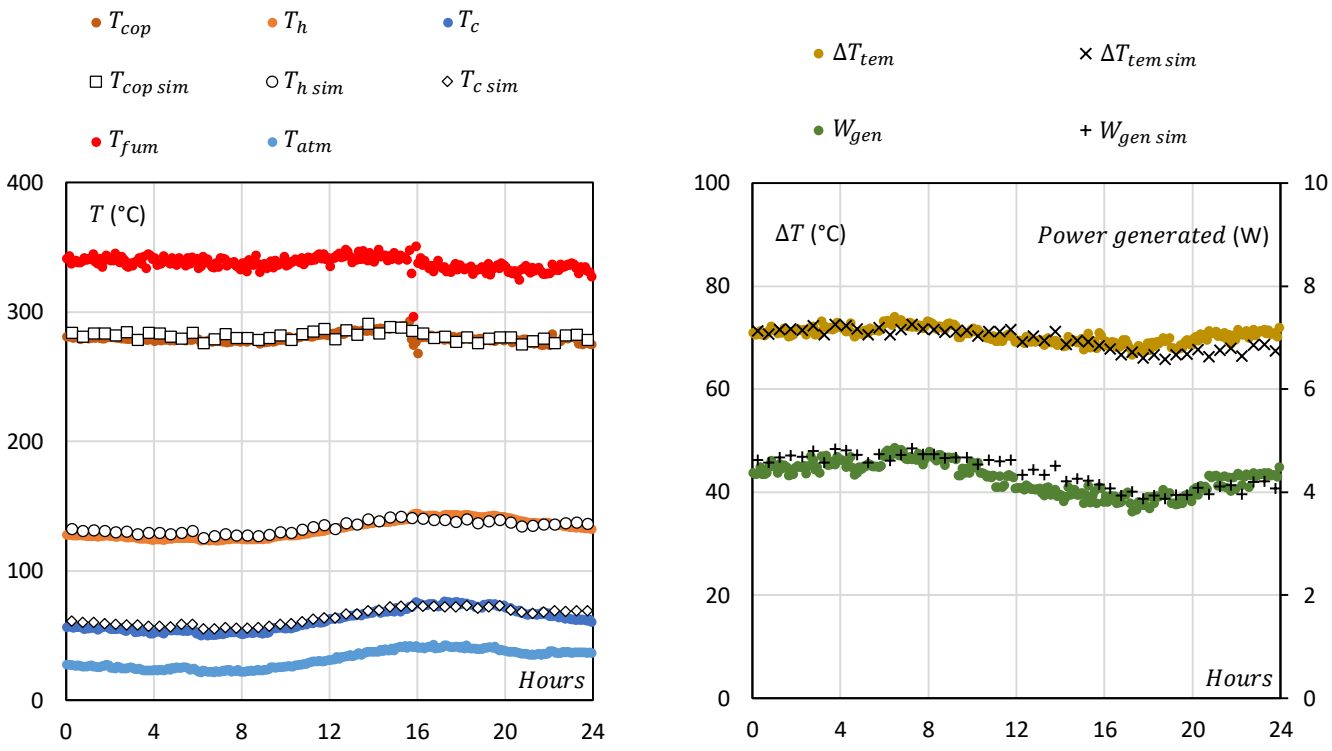

Figure 13: Temperature distribution and power generated during one sample day: Experimental and simulated data

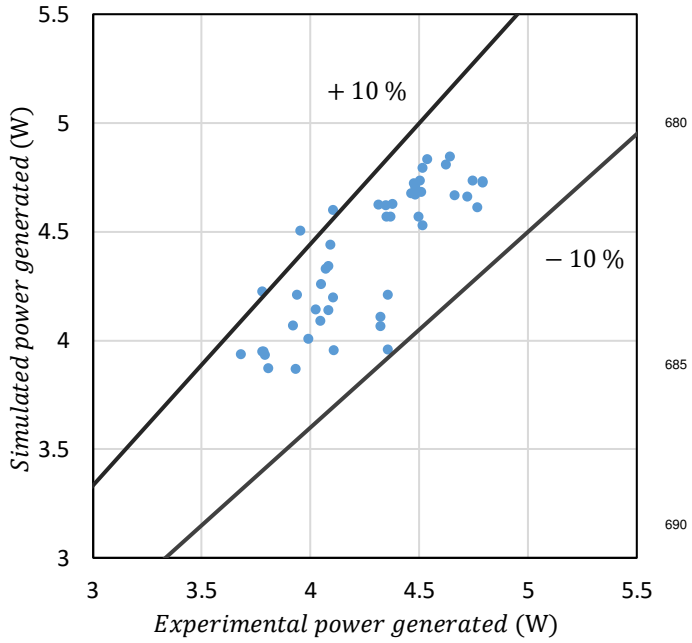

Figure 14: Simulated power generated by the TEG on the ±10 % experimental power range

be attached. As the temperature of the fumes drops power generated also decreases, at the first block, where the temperature of the fumes is at its highest, each TEG would produce 12.66 W, in contrast, at the last block 11.76 W would be produced. This system would be able to produce 30.8 MWh of energy during the whole year with 3.52 kW of average total output power and an efficiency of 2.89 %. The average Spanish household consumption of electricity is 3692 kWh over a year [32], therefore, the energy produced by the proposed system would be able to provide electricity to 8.34 average Spanish households each year.

6. Conclusions

A computational model that simulates the behaviour of a thermoelectric generator to harvest waste heat from hot fumes has been developed and used to optimize the configuration of the thermoelectric generator.

An experimental and computational study has been made in order to optimize the performance of the whole thermoelectric generator. Different cold side heat exchangers had been tested under laboratory conditions, as a result, Sintered type heat pipes with 5 mm fin spacing that lack moving parts outperformed the rest with a remarkably low thermal resistance of 0.255 K/W while dissipating 200 W of heat. A computational study has been performed of the optimal number of cold side heat exchangers and thermoelectric module for 1 hot side heat exchanger, the optimal configuration consists of 2 cold side heat exchangers and 4 thermoelectric modules (2 for cold side heat exchanger).

A thermoelectric generator with the optimized configuration suited to harvest energy in a rockwool manufacturing plant has been built, installed and tested at the manufacturing plant, acquiring experimental data during the 30 days field test period. Average power output during the testing period is 4.6 W with a 70.8 °C temperature gradient between the thermoelectric module faces and a 2.38 % efficiency. Using the experimental data obtained, the computational model is validated, as the relative error of the power generated stays between the ±10 %.

The harvesting potential when taking advantage of the whole pipe with an optimized design is calculated using the computational model. The proposed system consists of 288 optimized thermoelectric generators (1152 thermoelectric modules) and would be able to produce 30.8 MWh of energy during the whole year with 3.52 kW of average total output power and an efficiency of 2.89 %. This amount of energy could cover the electric consumption of 8.34 Spanish average households.

Acknowledgements

The authors are indebted to the Navarra Government for economic support of this work, included in the 0011-1365-2018-000101 Research Project, also to the State Research Agency of Spain for economic support, included in the RTI2018-093501-B-C22 Project from the Research Challenges Program. We would also like to acknowledge the support from the FPU Program of the Spanish Ministry of Science, Innovation and Universities (FPU16/05203).

References

[1] BP, BP statistical review of world energy 2018, Statistical Review of World Energy (2018) 40.

[2] J. Hansen, P. Kharecha, M. Sato, V. Masson-Delmotte, F. Ackerman, D. J. Beerling, P. J. Hearty, O. Hoegh-Guldberg, S. L. Hsu, C. Parmesan, J. Rockstrom, E. J. Rohling, J. Sachs, P. Smith, K. Steffen, L. Van Susteren, K. Von Schuckmann, J. C. Zachos, Assessing "dangerous climate change": Required reduction of carbon emissions to protect young people, future generations and nature, PLoS ONE 8 (12) (2013). doi:10.1371/journal.pone.0081648.

[3] S. C. Doney, V. J. Fabry, R. A. Feely, J. A. Kleypas, Ocean Acidification: The Other CO 2 Problem, Annual Review of Marine Science 1 (1) (2009) 169–192. doi:10.1146/annurev.marine.010908.163834.

[4] N. Armaroli, V. Balzani, The future of energy supply: Challenges and opportunities, Angewandte Chemie - International Edition 46 (1-2) (2007) 52–66. doi:10.1002/anie.200602373.

[5] Lawrence Livermore National Laboratory, U.S. Energy Flow Diagram 2018 (2018).
URL https://flowcharts.llnl.gov/content/assets/docs/2018{_}United-States{_}Energy.pdf

[6] C. Forman, I. K. Muritala, R. Pardemann, B. Meyer, Estimating the global waste heat potential, Renewable and Sustainable Energy Reviews 57 (2016) 1568–1579. doi:10.1016/j.rser.2015.12.192.
URL http://dx.doi.org/10.1016/j.rser.2015.12.192

[7] H. Jouhara, N. Khordehgah, S. Almahmoud, B. Delpech, A. Chauhan, S. A. Tassou, Waste heat recovery technologies and applications, Thermal Science and Engineering Progress 6 (April) (2018) 268–289. doi:10.1016/j.tsep.2018.04.017.
URL https://doi.org/10.1016/j.tsep.2018.04.017

[8] S. M. Pourkiaei, M. H. Ahmadi, M. Sadeghzadeh, S. Moosavi, F. Pourfayaz, L. Chen, M. A. Pour Yazdi, R. Kumar, Thermoelectric cooler and thermoelectric generator devices: A review of present and potential applications, modeling and materials, Energy 186 (2019) 115849. doi:10.1016/j.energy.2019.07.179.
URL https://doi.org/10.1016/j.energy.2019.07.179

[9] D. Zabek, F. Morini, Solid state generators and energy harvesters for waste heat recovery and thermal energy harvesting, Thermal Science and Engineering Progress 9 (November 2018) (2019) 235–247. doi:10.1016/j.tsep.2018.11.011.
URL https://doi.org/10.1016/j.tsep.2018.11.011

[10] T. C. Harman, J. M. Honig, Thermoelectric and thermomagnetic effects and applications, McGraw-Hill, 1967.

[11] P. Aranguren, D. Astrain, A. Rodríguez, A. Martínez, Experimental investigation of the applicability of a thermoelectric generator to recover waste heat from a combustion chamber, Applied Energy 152 (2015) 121–130. doi:10.1016/j.apenergy.2015.04.077.
URL http://dx.doi.org/10.1016/j.apenergy.2015.04.077

[12] P. Aranguren, M. Araiz, D. Astrain, Auxiliary consumption: A necessary energy that affects thermoelectric generation, Applied Thermal Engineering 141 (September 2017) (2018) 990–999. doi:10.1016/j.applthermaleng.2018.06.042.

[13] A. Kumar, K. Singh, R. Das, Response surface based experimental analysis and thermal resistance model of a thermoelectric power generation system, Applied Thermal Engineering 159 (May) (2019) 113935. doi:10.1016/j.applthermaleng.2019.113935.
URL https://doi.org/10.1016/j.applthermaleng.2019.113935

[14] L. Catalan, A. Garacochea, A. Casi, M. Araiz, P. Aranguren, D. Astrain, Experimental Evidence of the Viability of Thermoelectric Generators to Power Volcanic Monitoring Stations, Sensors (Basel, Switzerland) 20 (17) (2020). doi:10.3390/s20174839.

[15] J. Deng, F. Zhou, B. Shi, J. L. Torero, H. Qi, P. Liu, S. Ge, Z. Wang, C. Chen, Waste heat recovery, utilization and evaluation of coalfield fire applying heat pipe combined thermoelectric generator in Xinjiang, China, Energy 207 (2020). doi:10.1016/j.energy.2020.118303.

[16] P. Aranguren, D. Astrain, A. Rodríguez, A. Martínez, Net thermoelectric power generation improvement through heat transfer optimization, Applied Thermal Engineering 120 (2017) 496–505. doi:10.1016/j.applthermaleng.2017.04.022.
URL http://dx.doi.org/10.1016/j.applthermaleng.2017.04.022

[17] F. Meng, L. Chen, Y. Feng, B. Xiong, Thermoelectric generator for industrial gas phase waste heat recovery, Energy 135 (2017) 83–90. doi:10.1016/j.energy.2017.06.086.
URL http://dx.doi.org/10.1016/j.energy.2017.06.086

[18] K. Yazawa, A. Shakouri, T. J. Hendricks, Thermoelectric heat recovery from glass melt processes, Energy 118 (2017) 1035–1043. doi:10.1016/j.energy.2016.10.136.
URL http://dx.doi.org/10.1016/j.energy.2016.10.136

[19] R. Elankovan, S. Suresh, K. Karthick, M. M. M. Hussain, V. P. Chandramohan, Evaluation of thermoelectric power generated through waste heat recovery from long ducts and different thermal system configurations, Energy 185 (2019) 477–491. doi:10.1016/j.energy.2019.07.039.
URL https://doi.org/10.1016/j.energy.2019.07.039

[20] M. Araiz, Á. Casi, L. Catalán, Á. Martínez, D. Astrain, Prospects of waste-heat recovery from a real industry using thermoelectric generators: Economic and power output analysis, Energy Conversion and Management 205 (September 2019) (2020) 112376. doi:10.1016/j.enconman.2019.112376.
URL https://doi.org/10.1016/j.enconman.2019.112376

[21] M. Nesarajah, G. Frey, Optimized design of thermoelectric energy harvesting systems for waste heat recovery from exhaust pipes, Applied Sciences (Switzerland) 7 (6) (2017). doi:10.3390/app7060634.

[22] M. F. Remeli, A. Date, B. Orr, L. C. Ding, B. Singh, N. D. N. Affandi, A. Akbarzadeh, Experimental investigation of combined heat recovery and power generation using a heat pipe assisted thermoelectric generator system, Energy Conversion and Management 111 (2016) 147–157. doi:10.1016/j.enconman.2015.12.032.
URL http://dx.doi.org/10.1016/j.enconman.2015.12.

032

[23] P. Aranguren, M. Araiz, D. Astrain, A. Martínez, Thermoelectric generators for waste heat harvesting: A computational and experimental approach, Energy Conversion and Management 148 (2017) 680–691. doi:10.1016/j.enconman.2017.06.040.
URL http://dx.doi.org/10.1016/j.enconman.2017.06.040

[24] M. T. Børset, Ø. Wilhelmsen, S. Kjelstrup, O. S. Burheim, Exploring the potential for waste heat recovery during metal casting with thermoelectric generators: On-site experiments and mathematical modeling, Energy 118 (2017) 865–875. doi:10.1016/j.energy.2016.10.109.
URL http://dx.doi.org/10.1016/j.energy.2016.10.109

[25] A. Žukauskas, Heat transfer from Tubes in Crossflow, in: Advances in Heat Transfer, Academic Press, 1972.

[26] Marlow Industries, Technical Data Sheet for TG12-8 4–6.

[27] D. Astrain, J. G. Vián, A. Martínez, A. Rodríguez, Study of the influence of heat exchangers' thermal resistances on a thermoelectric generation system, Energy 35 (2) (2010) 602–610. doi:10.1016/j.energy.2009.10.031.

[28] A. Rodríguez, J. G. Vián, D. Astrain, A. Martínez, Study of thermoelectric systems applied to electric power generation, Energy Conversion and Management 50 (5) (2009) 1236–1243. doi:10.1016/j.enconman.2009.01.036.
URL http://dx.doi.org/10.1016/j.enconman.2009.01.036

[29] C. AJ, Heat transfer, 4th Edition, Macmillan, 1984.

[30] L. L. Vasiliev, Heat pipes in modern heat exchangers, Applied Thermal Engineering 25 (1) (2005) 1–19. doi:10.1016/j.applthermaleng.2003.12.004.

[31] Gobierno de Navarra, Meteo.Navarra.es (2019).
URL http://meteo.navarra.es/estaciones/estacion.cfm?IDEstacion=257

[32] P. SECH-SPAHOUSEC, Analyses of the energy consumption of the household sector in Spain (2011) 76.
URL www.cros-portal.eu/sites/default/files/SECH{_}Spain.pdf{%}5Cn